ACS APPLIED MATERIALS & INTERFACES

Research Article

www.acsami.org

Synthesis of Iron Oxide/Partly Graphitized Carbon Composites as a High-Efficiency and Low-Cost Cathode Catalyst for Microbial Fuel Cells

Ming Ma,[†,‡] Ying Dai,[†,§] Jin-long Zou,*[,†,‡] Lei Wang,[†] Kai Pan,[†] and Hong-gang Fu*[,†]

[†]Key Laboratory of Functional Inorganic Material Chemistry, Ministry of Education of the People's Republic of China, and [‡]Key Laboratory of Chemical Engineering Process and Technology for High-Efficiency Conversion, College of Heilongjiang Province, School of Chemistry and Materials Science, Heilongjiang University, Harbin 150080, China

[§]School of Civil Engineering, Heilongjiang Institute of Technology, Harbin 150050, China

Supporting Information

ABSTRACT: Waste cornstalks and pomelo skins are used as carbon resources for preparing nanocomposites of iron oxide and partly graphitized carbon (Fe_3O_4/PGC-CS and Fe_3O_4/PGC-PS). The results showed that Fe_3O_4 with a face-centered cubic structure is uniformly dispersed on the skeleton of Fe_3O_4/GC, and the highest S_{BET} values of Fe_3O_4/PGC-CS (476.5 m^2 g^{-1}) and Fe_3O_4/PGC-PS (547.7 m^2 g^{-1}) are obtained at 1000 °C. The electrical conductivity and density of catalytic active sites are correspondingly improved by the introduction of Fe species. Microbial fuel cells (MFCs) with a mixed composite (Fe_3O_4/PGC-CS:Fe_3O_4/PGC-PS = 1:1) cathode (three-dimensional structures) generate the highest power density of 1502 ± 30 mW m^{-2}, which is 26.01% higher than that of Pt/C (1192 ± 33 mW m^{-2}) and only declines by 7.12% after 18 cycles. The Fe_3O_4/PGC-CS cathode has the highest Coulombic efficiency (24.3 ± 0.7%). The Fe_3O_4/PGC composites exhibit high oxygen reduction reactivity, low charge transfer resistances, and long-term stability and can be used as a low-cost and high-efficiency catalyst for MFCs.

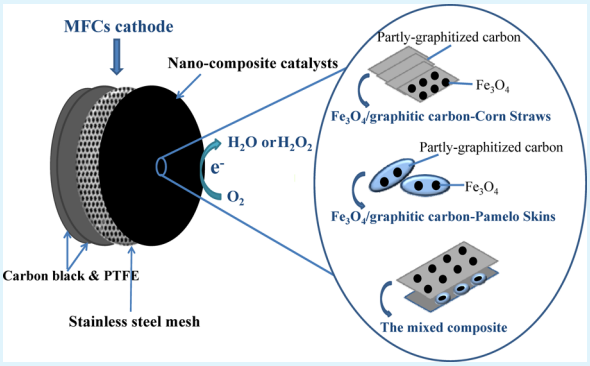

KEYWORDS: *graphitized carbon, microbial fuel cells, oxygen reduction reactivity, stability, waste biomass*

INTRODUCTION

Recently, a lot of attention has been paid to microbial fuel cells (MFCs) due to their potential use of electrochemically active microorganisms for clean, sustainable, renewable energy production associated with wastewater treatment.[1,2] In addition, new chemical production (hydrogen, methanol, ethanol, methane, and formate), CO_2 fixation, decolorization, desalination, and energy utilization in minisized MFCs for low-power-consumption niches (marine wireless sensors and implantable medical devices) are also appealing microbial electrochemical technologies.[3−6] However, the high power production cost has been a great challenge affecting the industrialization and commercial applications of MFC technology. The oxygen reduction reaction (ORR) as a kinetically slow process is undoubtedly the pivot among power density generation and investment of materials.[7,8] Specifically, more than 60% of the overall investment originates from the costs of cathode materials (i.e., support, catalyst, Nafion, and carbon black).[9] Platinum-based materials are the most widely used precious-metal catalysts for their superior ORR activity.[10] However, their susceptibility to CO poisoning and exorbitant price limit their large-scale application. Therefore, a novel, durable, highly active, and cheap catalyst has been desired in recent years.

New carbon materials with a unique structure and redox activity such as graphene and carbon nanotubes have been recognized as low-cost efficient catalysts.[11,12] Feng et al. used chemical vapor deposition (CVD) to synthesize nitrogen-doped carbon nanotubes (NCNTs) as MFC ORR cathode catalysts.[13] The vertical arrangement of the nanocluster structure of the CNTs diminished the internal resistance, then increased the cathode potential, and proceeded on a $4e^-$ pathway for efficient electrocatalysis in a neutral phosphate-buffered solution (PBS). The maximum power density (1600 ± 50 mW m^{-2}) and the stability were better than those of Pt/C (1393 ± 35 mW m^{-2}) after 25 cycles. Despite the complicated synthesis process, newly structured carbon has already become one of the most valuable substitutes in practical MFC applications due to its good ORR activity and high stability.[14]

Recent studies on ORR catalysts have shown that graphitized carbon nanostructured composites exhibit a relatively high

Received: April 1, 2014
Accepted: August 1, 2014
Published: August 1, 2014

electrocatalytic activity, electrical conductivity, and stability.[15,16] Transition metals were initially reported to show comparable catalytic activity for electroreduction of O_2 to Pt. For example, Su et al. synthesized a cobalt oxide/nitrogen-doped graphene (Co_3O_4/NG) nanocomposite by the hydrothermal method which showed high ORR and oxygen evolution reaction (OER) activities.[17] The power density was up to 1340 ± 10 mW m^{-2}, only a bit lower than that of Pt/C (1470 ± 10 mW m^{-2}). Hao Yu et al. prepared a series of Fe-based and Co-containing ORR catalysts that could be considered as a potential cathode choice for biological electricity generation.[18] Recently, Xia et al. used iron ethylenediaminetetraacetic acid solution to modify the activated carbon (MAC).[19] The electron donor capacity of this MAC had been enhanced by weakening teh O−O bond and was further improved by the transition metal Fe, which could stabilize the tetravalent nitrogen and promote the disproportionation of H_2O_2. It is generally recognized that the synergistic effect between the graphite carbon support and transition metal played a crucial role in the formation of active sites electrically conductive for ORR. However, considerable research is still required to solve the inherent problems associated with the complexity of the synthesis process, fallacious architecture, and poor interaction of graphite carbon and the active constituents.

In this paper, we report a method (one step) for preparation of Fe_3O_4/partly graphitized carbon (Fe_3O_4/PGC) by using two recycled biomasses (cornstalks and pomelo skins) which have a low cost and are easily accessible as carbon resources. Especially the carbonized fluffy spongelike skins of pomelo and straw could offer a high specific surface area, a great number of active sites, and a large pore volume for effective mass transport. The conductivity, catalytic activity, and stability of Fe_3O_4/PGC could be greatly enhanced by the introduction of a nano-Fe species, which was expected to have a higher ORR capacity in MFCs. The performance of the synthesized Fe_3O_4/PGC as the cathode catalyst in MFCs was compared with that of the commonly used Pt/C catalyst. The electrocatalytic activity of the Fe_3O_4/PGC for ORR in MFCs, which was still unknown, was also investigated in detail.

EXPERIMENTAL SECTION

Materials. Wasted cornstalks from farmland and residual pomelo skins were used as carbon resources for synthesis of carbon composites. After the outside crust of the cornstalks and pomelo skins (yellow skins) were stripped down, the inside cores were kept in desiccators for further use. Inocula used in this study were obtained from the effluent of the previous reactors that had been running for 4 months as previously described.[20] All chemicals used in the experiment were of analytical grade and were used without further purification.

Synthesis of Fe_3O_4/PGC Composites. The preparation of Fe_3O_4/PGC was conducted by using a simple in situ simultaneous synthesis method. Briefly, the spongelike parts of the cornstalks and pomelo skins were impregnated with $FeCl_3$ solution to form a carbon−Fe^{3+} complex with a mass ratio of 1:1. The resulting products were dried at 60 °C for 12 h in an oven and carbonized at 1000 °C for 1.5 h with a heating rate of 5 °C min^{-1} under a highly pure N_2 flow (50−60 mL min^{-1}). Finally, the black samples were ground into powder and washed with deionized water three times. The samples made from cornstalks and pomelo skins are designated as Fe_3O_4/PGC-PS and Fe_3O_4/PGC-CS, respectively. As a comparison, the above two products were washed with HCl (2 mol L^{-1}) for 12 h to completely remove the Fe species, and the resulting products are respectively designated as PGC-PS and PGC-CS.

Cathode Preparation for MFCs. The membrane-free single-chamber air-cathode MFCs were constructed by using a carbon fiber brush as the anode and stainless steel mesh as the cathode base material. The gas diffusion layer (GDL) of the air cathode was prepared by rolling carbon black and poly(tetrafluoroethylene) (PTFE) (60 wt %) with a mass ratio of 7:3 and then sintering the resulting material at 340 °C for 25 min. The catalyst layer was rolled onto the opposite side of the GDL with a mass ratio of 6:1 and the resulting material dried at 80 °C according to the previously reported method.[21] Five kinds of carbon-based cathodes were prepared, including Fe_3O_4/PGC-PS and Fe_3O_4/PGC-CS and their physical mixture (at a mass ratio of 1:1; Figure S1, Supporting Information), PGC-PS, and PGC-CS. For comparison, commercially available Pt/C (10 wt %) powder was also used as the cathode catalyst (5 mg cm^{-2}).

MFC Configuration and Operation. MFCs were conducted with single-chamber reactors 4 cm long and 3 cm in diameter as previously described in the literature.[22] The graphite fiber brush anode was pretreated with acetone and heated in the air. All the reactors were inoculated by using the effluent from MFCs operated for 4 months, and operated at a fixed external circuit resistance (1000 Ω). The substrate solution contained glucose (1 g L^{-1}) and PBS, which contained NH_4Cl (0.31 g L^{-1}), $NaH_2PO_4{\cdot}2H_2O$ (3.321 g L^{-1}), $Na_2HPO_4{\cdot}12H_2O$ (10.3174 g L^{-1}), KCl (0.13 g L^{-1}), trace minerals (12.5 mL L^{-1}), and vitamins (5 mL L^{-1}).[23] The MFC operating temperature was maintained at 30 °C, and the medium was replaced with the fuel when the voltage decreased to less than 50 mV, which formed one complete cycle. To achieve statistical soundness, at least two replicates were carried out.

Materials Characterization. X-ray diffraction (XRD) patterns were collected with a Rigaku D/max-IIIB diffractometer using Cu Kα radiation (λ = 1.5406 Å) at step scan of 0.02° from 10° to 80°. The voltage and the applied current were 40 kV and 20 mA, respectively. The resulting powder diffraction patterns were analyzed according to the Joint Committee on Powder Diffraction Standard data. Raman spectra were recorded with an HR 800 micro Raman spectrometer (Jobin-Yvon, France) at 457.9 nm. The laser beam was focused on the sample with a 50× objective. The laser intensity excited by an argon ion laser was kept below the threshold for any laser-induced changes in the Raman spectra or electrical transport. Transmission electron microscopy (TEM) images were taken by using a JEM-2100 electron microscope (JEOL) with an acceleration voltage of 200 kV. The nitrogen adsorption/desorption isotherms were measured at 77 K using a Micromeritics Tristar II. The specific surface area of the materials was calculated by the Brunauer−Emmett−Teller (BET) theory. The pore size distribution was computed by using the Barrett−Joyner−Halenda (BJH) method from the adsorption branch of the isotherm. Thermogravimetry (TG) and differential scanning calorimetry (DSC) experiments were carried out with a TA Instruments (NEJSCH STA 449C) simultaneous DSC−TGA apparatus. The powder sample was heated from 30 to 1000 °C at 5 °C min^{-1} in an O_2 atmosphere with a flow rate of 60 mL min^{-1}.

Electrochemical Analysis. Electrochemical measurements were conducted on a computer-controlled electrochemical workstation (BAS100B electrochemical workstation, Germany) with a typical three-electrode cell equipped with gas flow systems.[24] Linear sweep voltammetry (LSV) was performed at 1 mV s^{-1} on the cathodes, and the reactor was filled with 28 mL of 50 mM PBS solution and equipped with a 2.25 cm^2 platinum sheet square counter electrode and a Ag/AgCl reference electrode (+0.195 V vs the standard hydrogen electrode, 3.0 M KCl). The cyclic voltammetry (CV) scan was performed in the potential range of −0.6 to +0.4 V at a scan rate of 10 mV s^{-1}.

A rotating disk electrode (RDE) can be used to explore the mechanism of the complex electrode reaction and obtain more information on the catalyst properties. Therefore, RDE tests were conducted to evaluate the catalyst activity of the Fe_3O_4/PGC composites by comparison with that of Pt/C. The RDE type used for ORR measurements was a glassy carbon rotating disk electrode, which was 0.4 cm in diameter (the effective disk area was 0.126 cm^2). Catalyst ink was prepared by adding a 10 mg powdered sample to 10 mL of isopropyl alcohol, and the resulting solution was then treated ultrasonically for 15 min. The ink suspension (10 μL) was dropped onto a 0.4 cm diameter glassy carbon electrode and dried in the air

until formation of a uniform film (sample loading of 0.079 mg cm^{-2}). Nafion (5 wt % solution, 5 μL) was then added to the coated catalyst for kinetic analysis. The RDE tests were carried out by using a modulated speed rotator (BAS Inc. Japan) immersed in a medium of 50 mM PBS at rotation rates of 400−3600 rpm with a pure oxygen flow. The solutions should be sparged with O_2 for at least 30 min. The average number of transferred electrons (n) and kinetic current (i_K) for the oxygen reduction reaction were calculated on the basis of the Koutecky−Levich (K−L) equation:[25]

$$\frac{1}{i} = \frac{1}{i_K} + \left(\frac{1}{0.62nFAD^{2/3}\nu^{-1/6}C}\right)\omega^{-1/2}$$

where i is the measured current (A), F is the Faraday constant (96 485 C mol^{-1}), A is the effective projected area of the disk electrode (0.126 cm^2, 0.4 cm in diameter), D is the diffusion coefficient of oxygen (2.7×10^{-5} cm^2 s^{-1}), ν is the kinematic viscosity (8.08×10^{-3} cm^2 s^{-1}), C is the concentration of oxygen in the solution (2.3×10^{-7} mol cm^{-3}), and ω is the rotation rate of the electrode.

Electrochemical impedance spectroscopy (EIS) was conducted at the open circuit voltage (OCV) over a frequency range of 10^5 to 10^{-2} Hz with a sinusoidal perturbation of 10 mV amplitude. EIS data were analyzed by fitting the spectra to an equivalent circuit model (Figure S2, Supporting Information). The produced voltage (E_{cell}) and electrode potentials were measured at a fixed external circuit resistance (1000 Ω) by using a multimeter and Ag/AgCl reference electrode. After the reactors were operated with fresh substrate for about 2 h, polarization and power density curves were obtained by measuring the stable voltage generated at various external resistances (50−5000 Ω). All the other parameters, including current density, power density, and Coulombic efficiency (CE), were calculated from the ratio of the total electrical charge produced within every cycle at different external resistances to the theoretical amount of electrons available from the oxidation of glucose to carbon dioxide. All the above electrochemical experiments were carried out at 30 °C. The chemical oxygen demand (COD) in MFCs was determined by the potassium dichromate oxidation method.

RESULTS AND DISCUSSION

Characteristics Analyses of Fe_3O_4/PGC Composites. As shown in Figure 1, the XRD patterns of Fe_3O_4/PGC-CS and Fe_3O_4/PGC-PS carbonized at 900−1050 °C were almost the same. The typical crystalline phases of the two composites carbonized at 900 °C were Fe_3O_4 nanoparticles (JCPDS card no. 75-1609) with a face-centered cubic structure (30°, 35.4°, 43°, 53.4°, 56.9°, and 62.5°). At 950, 1000, and 1050 °C, the peaks at 44.5° corresponded to the typical diffraction peaks of α-Fe with a body-centered cubic structure, which was the main difference from those at 900 °C. This implied that, at higher temperatures, part of the Fe_3O_4 particles in Fe_3O_4/PGC composites were reduced to α-Fe by in situ carbothermal reduction. At 1050 °C, the graphitized carbon (26.2°), which originated from the carbon graphitization catalyzed by iron species, was obviously detected in the two Fe_3O_4/PGC composites. The graphitization of carbon was a gradual and slow process, which means that the PGC was already present in the Fe_3O_4/PGC composites at 950 or 1000 °C.

Figure 2 shows the Raman spectra of Fe_3O_4/PGC-CS and Fe_3O_4/PGC-PS carbonized at 900−1050 °C. As the temperature increased, the I_G/I_D (the D and G bands usually correspond to the sp^3 defect sites and the bond stretching of sp^2-bonded pairs, respectively) value increased gradually, which means that the graphitization degree of Fe_3O_4/PGC-CS or Fe_3O_4/PGC-PS was increased.[26] Meanwhile, the peak for the G bands of Fe_3O_4/PGC-CS (Figure 2A) was transferred from 1588 cm^{-1} (900 °C) to 1576 cm^{-1} (1050 °C); for Fe_3O_4/PGC-PS (Figure 2B), the peak was transferred from 1582 cm^{-1} (900 °C) to 1570 cm^{-1} (1050 °C). The peak shift for the G bands of Fe_3O_4/PGC-PS (10 cm^{-1}) was higher than that of Fe_3O_4/PGC-CS (4 cm^{-1}), taking the highly oriented pyrolytic graphite (1580 cm^{-1}) as the standard. This implies that the greater the

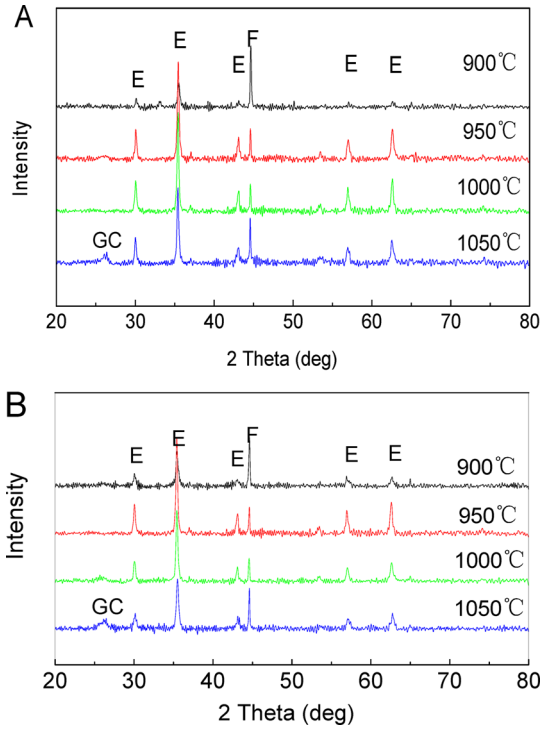

Figure 1. XRD analyses of the main crystalline phases (E, Fe_3O_4; F, α-Fe; GC, graphited carbon) in Fe_3O_4/PGC-CS (A) and Fe_3O_4/PGC-PS (B) carbonized at 900−1050 °C.

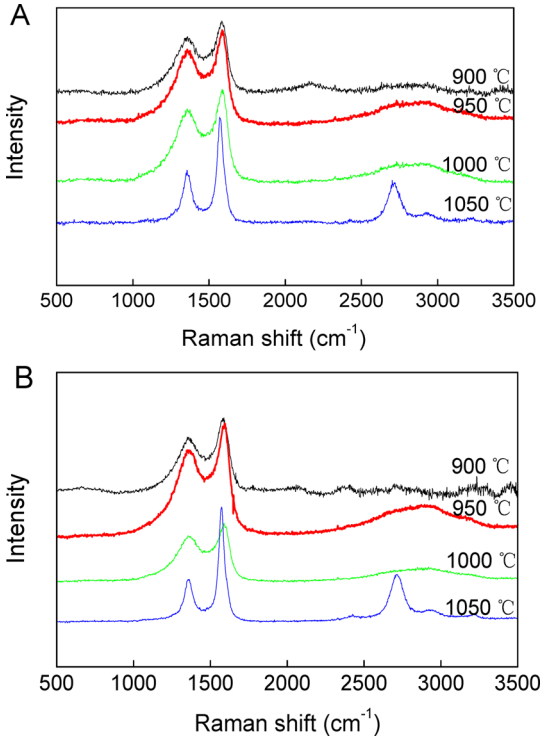

Figure 2. Raman spectrum of Fe_3O_4/PGC-CS (A) and Fe_3O_4/PGC-PS (B) carbonized at 900−1050 °C.

dx.doi.org/10.1021/am501844p | ACS Appl. Mater. Interfaces 2014, 6, 13438−13447

shift of the G bands to lower wavenumber, the higher the degree of carbon curling.[27]

N_2 adsorption−desorption isotherms and pore size distribution curves of Fe_3O_4/PGC-CS and Fe_3O_4/PGC-PS carbonized at 900−1050 °C are shown in Figures S3 and S4 (Supporting Information), respectively. It can be seen that both Fe_3O_4/PGC-CS and Fe_3O_4/PGC-PS showed typical type IV isotherms with a sharp capillary condensation step and H2-type hysteresis loops at relative pressures of 0.5−0.8. Their pore size distributions were very wide and mainly consisted of mesopores, and the average pore size decreased gradually as the temperature increased (Figures S3 and S4). The highest S_{BET} values of Fe_3O_4/PGC-CS (476.5 m^2 g^{-1}) and Fe_3O_4/PGC-PS (547.7 m^2 g^{-1}) were both obtained at 1000 °C, which showed that the development of the porous structure of the composite made from pomelo skins was better than that from cornstalks (Table 1). One reason was that the structure of the spongelike part of pomelo skins was quite different from that of cornstalks, which resulted in the difference in S_{BET}.

Table 1. Textural Properties of Fe_3O_4/PGC-CS and Fe_3O_4/PGC-PS Obtained at 900−1050 °C

sample	surface area/m^2 g^{-1}	pore vol/cm^3 g^{-1}	av pore width/nm
Fe_3O_4/PGC-CS-900	391.22	0.22	12.59
Fe_3O_4/PGC-CS-950	400.86	0.19	12.13
Fe_3O_4/PGC-CS-1000	476.55	0.27	11.31
Fe_3O_4/PGC-CS-1050	382.01	0.26	10.75
Fe_3O_4/PGC-PS-900	371.78	0.25	10.63
Fe_3O_4/PGC-PS-950	482.68	0.29	10.69
Fe_3O_4/PGC-PS-1000	545.95	0.34	9.85
Fe_3O_4/PGC-PS-1050	265.92	0.14	8.77

According to the above analyses, 1000 °C was selected as the optimal temperature for Fe_3O_4/PGC composite preparation. The morphological features of Fe_3O_4/PGC-CS and Fe_3O_4/PGC-PS carbonized at 1000 °C were observed by TEM (Figure 3). Fe_3O_4 with particle sizes of 10−20 nm was uniformly distributed in Fe_3O_4/PGC-CS, and no agglomeration phenomena are observed in Figure 3A. Figure 3B shows that the GC was already formed in the body of Fe_3O_4/PGC-CS and tightly surrounded the Fe_3O_4 particles. As observed in Figure 3D,E, some of the aggregated Fe_3O_4 particles were connected tightly to each other and inlaid in the nanocapsule structure of Fe_3O_4/PGC-PS. The conductivity and electron transfer of the Fe_3O_4/PGC composites were inevitably enhanced by the high degree of carbon graphitization.[15,16] As shown in Figure 3C,F, the lattice spacing marked in the pattern between the (311) planes of Fe_3O_4 was 0.25 nm (HRTEM measurements). The cathodes made with the stable Fe_3O_4/PGC composites were expected to have multiple catalytic active sites and high electrocatalytic activity.

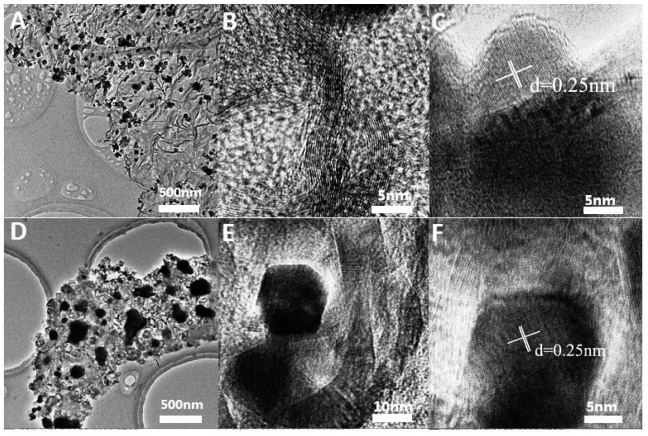

Figure 3. TEM image of Fe_3O_4/PGC-CS (A), HRTEM images of PGC-CS (B), and HRTEM images of Fe_3O_4 (C) for Fe_3O_4/PGC-CS. TEM image of Fe_3O_4/PGC-PS (D), HRTEM images of PGC-CS (E), and HRTEM images of Fe_3O_4 (F) for Fe_3O_4/PGC-CS.

Simultaneous TG−DSC analyses of Fe_3O_4/PGC-CS and Fe_3O_4/PGC-PS are shown in Figure 4. The exothermic process

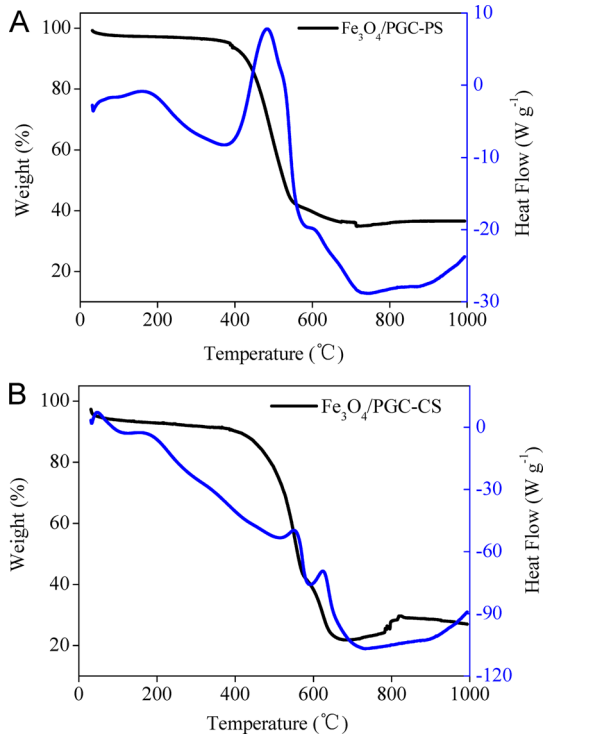

Figure 4. Thermogravimetry and differential scanning calorimetry (TG−DSC) analyses of Fe_3O_4/PGC-PS (A) and Fe_3O_4/PGC-CS (B).

with a corresponding weight loss of 65% appeared in the range of 400−720 °C, which should be attributed to the burning loss of carbon (in the form of CO_2 or CO) from Fe_3O_4/PGC-PS (Figure 4A). The corresponding weight loss of 80% for Fe_3O_4/PGC-CS occurred in the range of 420−660 °C (Figure 4B). These results suggest that the content of Fe species in Fe_3O_4/PGC-PS (about 35%) was higher than that of Fe_3O_4/PGC-CS (about 20%), which could be attributed to the different complexing capacities of Fe^{3+} and the carbon resource.

MFC Performance of Fe_3O_4/PGC Composite Cathodes. LSV scan tests for the cathode materials (Figure S5, Supporting Information) showed that the mixture cathode of Fe_3O_4/PGC-CS and Fe_3O_4/PGC-PS (mass ratio of 1:1) had the highest current density in the potential range of −1.5 to +0.4 V vs the Ag/AgCl reference electrode. The unique highly porous stack structures of the mixture made it more favorable for chemisorption of oxygen onto the catalyst surface, which inevitably enhanced the ORR electrocatalytic activity.[28] Fe_3O_4/PGC-CS cathodes produced a slightly higher current density than Fe_3O_4/GC-PS cathodes. To further evaluate the ORR

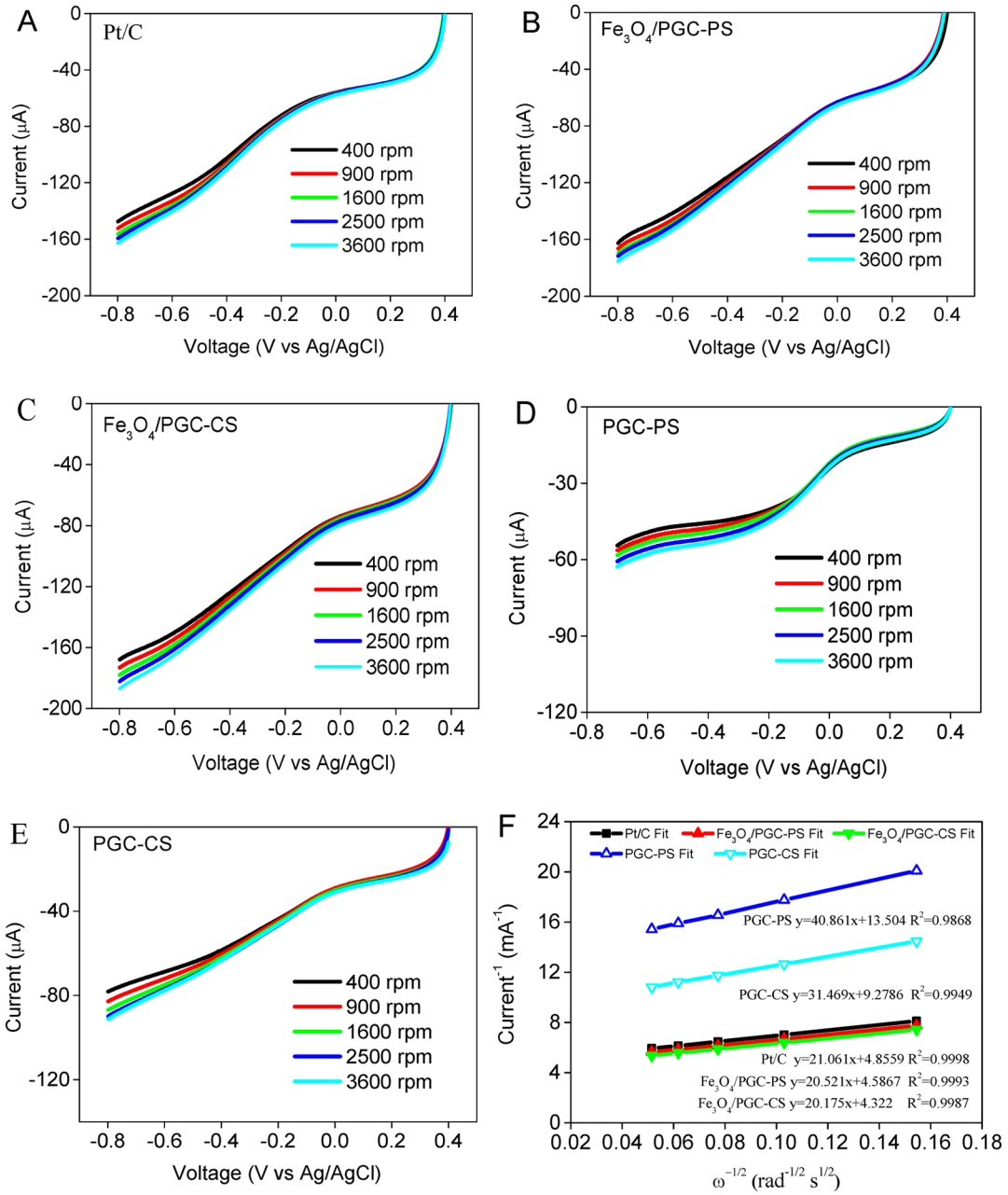

Figure 5. Rotating disk electrode test of catalyst inks with (A) Pt/C, (B) Fe_3O_4/PGC-PS, (C) Fe_3O_4/PGC-CS, (D) PGC-PS, and (E) PGC-CS collected at rotation rates from 400 to 3600 rpm. (F) Koutecky–Levich analysis of oxygen reduction on different catalysts.

electrocatalytic activity, CV tests of different cathodes in 50 mM PBS saturated with O_2 and N_2 were conducted. As shown in Figure S6 (Supporting Information), PGC-PS and PGC-CS exhibited a weaker current response and also showed poor catalytic activity for ORR, and PGC-PS had a minimum current of 7.43 mA in O_2-saturated solution (Figure S7A, Supporting Information). The current of Fe_3O_4/PGC-CS (13.84 mA) was higher than that of Fe_3O_4/PGC-PS (11.96 mA), which might be due to the large surface area, high conductivity, and excellent ORR activity of the Fe_3O_4/PGC-CS composite.[15,16] The current values for Fe_3O_4/PGC composites were higher than that of Pt/C (10.82 mA). A significant decrease in current generation happened in the N_2-saturated solution test (Figure S7B). It should be noted that the redox peaks were unobvious in this study, consistent with the previously reported results,[29] which might be attributed to the confines of CV testing methods for MFCs.

To examine the ORR kinetic current and the transferred electron number, RDE was tested in 50 mM O_2-saturated PBS at rotation rates of 400–3600 rpm. At the highest rotation rate (3600 rpm), Fe_3O_4/PGC-CS generated the highest limiting current of 0.186 mA, which was slightly higher than that of Fe_3O_4/PGC-PS (0.177 mA) and 10.06% higher than that of Pt/C (0.169 mA) (Figure 5A–C). The lowest limiting current (0.065 mA) was generated by PGC-PS, which indicated that Fe_3O_4 could be the important active functional site for ORR (Figure 5D,E). The kinetic current of different catalysts was calculated by the K–L equation (Figure 5F) and was 0.23, 0.22, 0.21, 0.11, and 0.07 mA for Fe_3O_4/PGC-CS, Fe_3O_4/PGC-PS, Pt/C, PGC-CS, and PGC-PS, respectively. The average number (n) of transferred electrons on Fe_3O_4/PGC-CS and Fe_3O_4/

dx.doi.org/10.1021/am501844p | ACS Appl. Mater. Interfaces 2014, 6, 13438–13447

PGC-PS was 3.70 and 3.61, respectively, which indicates the dominant pathway for ORR was the four-electron oxygen reduction, including Pt/C (n = 3.56). Additionally, Fe_3O_4-free PGC-CS (n = 2.5) and PGC-PS (n = 2.0) exhibited much poorer ORR activity, suggesting the presence of a two-electron ORR pathway on PGC. The Fe_3O_4/PGC composites afforded higher ORR activity than PGC composites due to the comparable synergistic catalytic activities of nano-Fe_3O_4 particles and PGC. The RDE results were consistent with those observed in CV scans, which could confirm the better ORR activity of the prepared composites.

Generally, the ORR activity was inevitably related to the unique structure and properties of the catalysts.[24,25] The superior electrocatalytic activity obtained here was due to the synergistic effect of PGC and Fe_3O_4 nanoparticles. The size of the Fe_3O_4 nanoparticles (10−20 nm in diameter) obtained here was smaller than the previously reported 110 and 150 nm,[30,31] which could improve the migration of oxygen atoms between PGC and Fe_3O_4 and provide a large surface area and various active sites for ORR. Furthermore, the carbon resources were derived from natural biomass, which was favorable for generating abundant oxygen-containing functional groups in PGC. All these factors made the complete oxygen reduction occur more easily in the four-electron pathway on Fe_3O_4/PGC composites. Two-electron ORR occurred on PGC in which oxygen was mainly reduced to H_2O_2 when catalyzed by pure carbon without an active metal component.[21]

As shown in Figure 6, EIS was used to investigate the kinetic activities on the cathodes,[32] and the diameters in the semicircles developed with Nyquist plots indicated that the charge transfer resistances (R_{ct}) of the Fe_3O_4/PGC-PS (15.3 ± 0.2 Ω) and Fe_3O_4/PGC-CS (10.8 ± 0.3 Ω) electrodes were lower than that of Pt/C (18.1 ± 0.5 Ω) and 52.79% and 62.45% lower than those of PGC-PS (32.2 ± 0.2 Ω) and PGC-CS (28.76 ± 0.3 Ω), respectively (Figure 6, Table 2). The decrease in charge transfer resistance verified the hypothesis that the introduction of Fe species could enhance the conductivity, electron transportation, and entire ORR performance of the composites.[15,16] Furthermore, the density of catalytic active sites could be effectively improved by the uniform distribution of Fe species in the PGC skeleton. The R_{ct} value of the mixture cathode (7.2 ± 0.2 Ω) was the lowest one, which was probably caused by the parallel arrangement of two resistors (Fe_3O_4/PGC-PS and Fe_3O_4/PGC-CS).

As shown in Figure S7 (Supporting Information), the voltage output of MFCs with the mixed cathode was higher than those of the other five cathodes. The voltage output of all MFCs at a fixed resistance (1000 Ω) gradually decreased after 800 h due to the formation of a biofilm on the cathode surface. It can be seen from Figure 7A that the average maximum voltage output of MFCs with the mixed cathode (0.64 ± 0.03 V) over the 21 feeding cycles was the highest. The voltage outputs of Fe_3O_4/PGC-PS (0.61 ± 0.04 V) and Fe_3O_4/PGC-CS (0.61 ± 0.02 V) were almost the same and were slightly higher than that of Pt/C (0.58 ± 0.05 V) and 52.13% and 37.54% higher than those of PGC-PS (0.292 ± 0.02 V) and PGC-CS (0.381 ± 0.04 V), respectively. By using the same anodes, the properties of the cathodes were dramatically influenced by the oxygen permeability and biofilm grown on the solution side of the cathodes. Three-dimensional structures of the mixed cathode were constructed by mixing 50% Fe_3O_4/PGC-CS and 50% Fe_3O_4/PGC-PS, which was favorable for ORR activity and antibiotic carbon. The Coulombic efficiencies (CEs) and COD

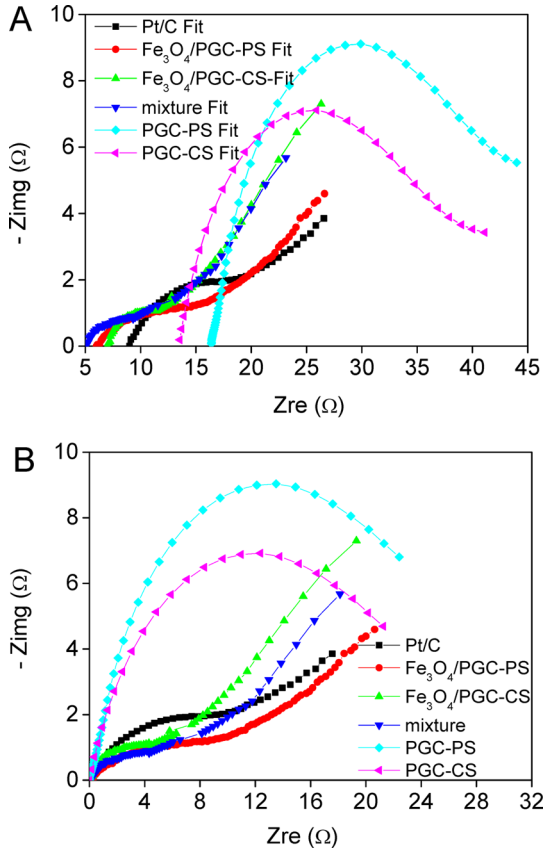

Figure 6. (A) Nyquist plots of Pt/C, Fe_3O_4/PGC-PS, Fe_3O_4/PGC-CS, a mixture of the two composites, PGC-PS, and PGC-CS. (B) Nyquist plots with the Z_{re} axis shifted to zero for comparison of charge transfer resistances of Pt/C, Fe_3O_4/PGC-PS, Fe_3O_4/PGC-CS, a mixture of the two composites, PGC-PS, and PGC-CS.

removal rates of MFCs with Fe_3O_4/PGC-CS were slightly higher (about 5%) than those of Pt/C and almost the same as those of the other two cathodes (Figure 7B). Although the voltage output of MFCs with the mixture cathode was the highest, this did not mean that the CEs related to the electronic recycling efficiency must be high.

Because the stability of long-term operation was one of the most significant indicators of the performance of MFCs,[33] the power density and corresponding electrode potentials of four catalysts were tested in the initial and final cycles (Figure 8). In the initial cycle (Figure 8A), the OCV for the mixture cathode was about 0.85 ± 0.05 V, and the mixture cathode showed the highest power density of 1502 ± 30 mW m^{-2}, which was about 4.09% and 12.26% higher than those of Fe_3O_4/PGC-CS (1443 ± 63 mW m^{-2}, 0.80 ± 0.02 V) and Fe_3O_4/PGC-PS (1338 ± 86 mW m^{-2}, 0.79 ± 0.02 V), respectively. The electricity production capacities for the mixture, Fe_3O_4/PGC-CS, and Fe_3O_4/PGC-PS were all better than that of Pt/C (1192 ± 33 mW m^{-2}, 0.77 ± 0.02 V) and extremely superior to those of PGC-PS (292 ± 21 mW m^{-2}, 0.51 ± 0.02 V) and PGC-CS (381 ± 23 mW m^{-2}, 0.54 ± 0.05 V), consistent with the voltage output (Figure 7A). Figure 8B shows the unobvious change of the anode potential and distinctive variations of the cathode potential as the current density increased, which suggests that the difference in power generation is attributed to the different ORR properties of the cathode.[34] The maximum power density obtained by this mixture cathode was higher than that of the

Table 2. Electrochemical Impedance Fitting Results of Different Cathodes

param	Pt/C	Fe_3O_4/PGC-PS	Fe_3O_4/PGC-CS	mixture	PGC-PS	PGC-CS
R_s (Ω)	9.86	6.42	7.81	5.15	16.87	13.86
R_{ct} (Ω)	18.1 ± 0.5	15.3 ± 0.2	10.8 ± 0.3	7.2 ± 0.2	32.2 ± 0.2	28.76 ± 0.3
Z_w ($\Omega \cdot s^{-1/2}$)	3.86×10^{-13}	4.23×10^{-13}	6.89×10^{-13}	3.25×10^{-13}	7.79×10^{-14}	8.64×10^{-14}
Q ($F \cdot s^{n-1}$)	7.77×10^{-3}	7.81×10^{-3}	4.68×10^{-3}	6.57×10^{-3}	8.83×10^{-3}	8.93×10^{-3}
n	0.78	0.56	0.71	0.52	0.98	0.88

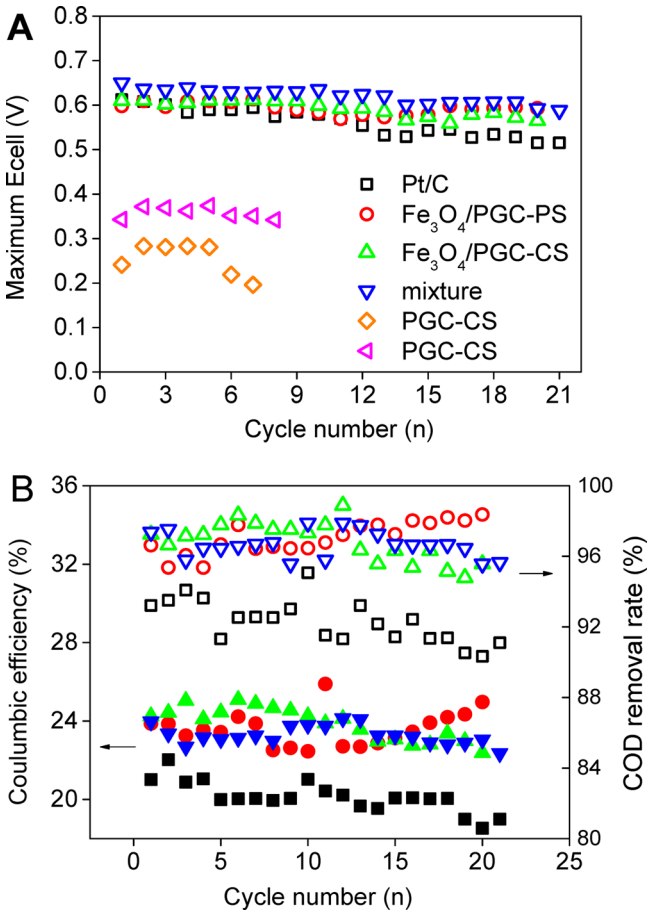

Figure 7. (A) Maximum cell voltage of each cycle for cathodes of Pt/C, Fe_3O_4/PGC-PS, Fe_3O_4/PGC-CS, a mixture of the two composites, PGC-PS, and PGC-CS. (B) Coulombic efficiency and COD removal rate of reactors with cathodes of Pt/C, Fe_3O_4/PGC-PS, Fe_3O_4/PGC-CS, and a mixture of the two composites.

Co_3O_4/stainless steel mesh or Fe/Fe_3C/C nanorod cathode catalyst reported previously.[35,36]

After the 18th cycle (Figure 8C,D), the highest power density (1395 ± 46 mW m^{-2}, 0.82 ± 0.06 V) was still obtained by the mixed composite cathode, and it only slightly declined by 7.12%, which was lower than that (17.0%) of Pt/C (989 ± 81 mW m^{-2}, 0.71 ± 0.02 V). The power density of the Fe_3O_4/PGC-CS and Fe_3O_4/PGC-PS reactors declined by 16.9% (1182 ± 5 mW m^{-2}, 0.78 ± 0.02 V) and 10.2% (1202 ± 67 mW m^{-2}, 0.71 ± 0.01 V), respectively. The decline of the power density for Pt/C, Fe_3O_4/PGC-CS, and Fe_3O_4/PGC-PS was higher than that of the mixed composites, which was attributed to the higher oxygen permeability and greater biofilm growth. For the mixed composite cathode, biofilm growth might be slower than that of the Pt/C cathode because it was thick enough for inhibiting oxygen permeability (~0.5 mm for the mixed composite cathode and ~0.15 mm for Pt/C). Besides, the Fe_3O_4/PGC-CS samples were much looser than the Fe_3O_4/PGC-PS samples, which led to a similar increase of thickness of the Fe_3O_4/PGC-CS cathode. Therefore, the power density of Fe_3O_4/PGC-CS was slightly better than that of Fe_3O_4/PGC-PS in the initial operation stage, but declined rapidly in the next operations, consistent with the change of electricity production (Figure 7A) and electronics utilization (Figure 7B). Generally, good oxygen permeability was favorable for ORR and unfavorable for inhibiting the growth of bacteria.[37] A balance of these two effects could be achieved by the mixture cathode, which had the highest power density and stability.

As shown in Figure 9, the CE of the Fe_3O_4/PGC-PS cathode varied in a wide range of 25−61% as the current density increased from 0.82 to 5.4 A m^{-2}, which was higher than that of Pt/C (20−50%) over the same range of current densities and slightly higher than those of the mixture (23−55%, 0.88−6.1 A m^{-2}) and Fe_3O_4/GC-CS (23−55%, 0.89−4.6 A m^{-2}). It was interesting that the mixed cathode for MFCs had the highest power density output, while the Fe_3O_4/PGC-CS and Fe_3O_4/PGC-PS cathodes had the highest CEs (vs cycles and vs current densities, respectivley). The Fe_3O_4/PGC composite cathode could efficiently decrease the ORR overpotential and improve the interfacial contact for proton transport.[38] Besides, the gradually graphitized accumulation process provided smaller, highly dispersed, and sufficient surface active sites for ORR.[39] However, they could also be attacked by peroxide radicals (H_2O_2) formed on the surface of teh three-phase boundary via insufficient ORR progress, which could also have an adverse effect on mass transfer and stability.[40] From this perspective, the actual work number of catalytic active sites of the nano-Fe_3O_4/PGC composites was larger than that of the commercial Pt/C catalyst. Therefore, the Fe_3O_4/PGC composite or mixture could be used as an alternative MFC cathode catalyst for its high-efficiency and low-cost electricity production without losing power efficiency and stability.

CONCLUSIONS

Nano-Fe_3O_4/PGC composites including Fe_3O_4/PGC-CS and Fe_3O_4/PGC-PS were synthesized from waste agricultural biomass (cornstalks and pomelo skins) via the in situ simultaneous reduction method. The electrochemical properties of Fe_3O_4/PGC used in single air-cathode microbial fuel cells (MFCs) as cathode catalysts were examined. The results showed that the Fe_3O_4/PGC composites exhibited high electrocatalysis activity for ORR. High-efficiency electricity generation could be obtained in MFCs with the Fe_3O_4/PGC and mixture cathodes and was more economical and sustainable than that with the Pt/C cathode. The Fe_3O_4/PGC composites, by reutilization of low-cost carbon resources, could be promising catalysts for practical application and commercialization of MFCs.

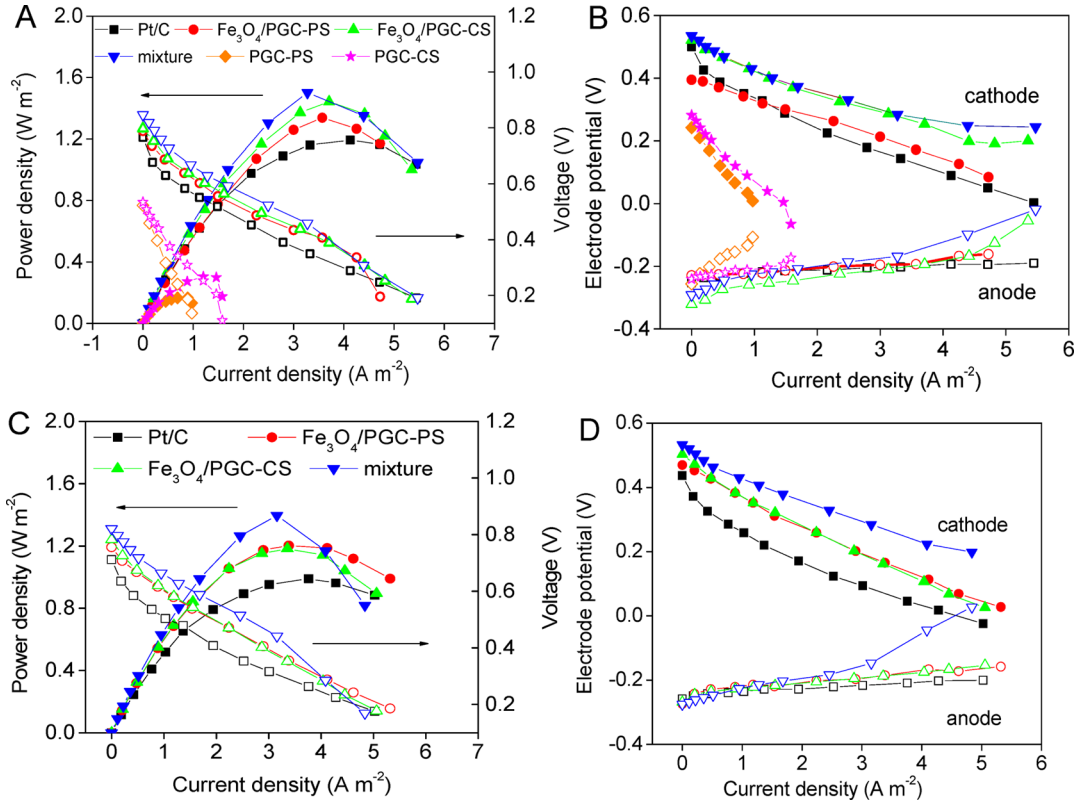

Figure 8. Power density and the corresponding electrode potentials using different cathodes as a function of the current density at the 4th cycle (A, B; the cathodes include Pt/C, Fe_3O_4/PGC-PS, Fe_3O_4/PGC-CS, a mixture of the two composites, PGC-PS, and PGC-CS) and the 18th cycle (C, D; the cathodes include Pt/C, Fe_3O_4/PGC-PS, Fe_3O_4/PGC-CS, and a mixture of the two composites).

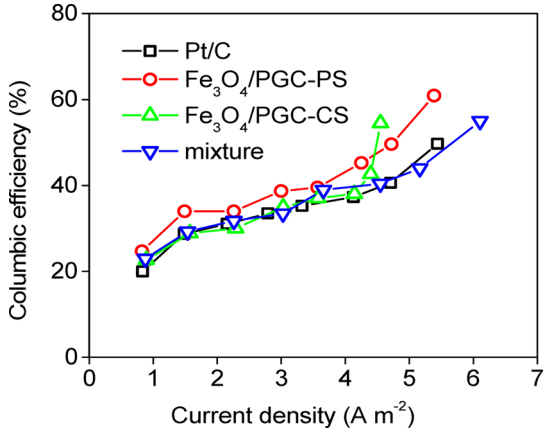

Figure 9. Relationship of Coulombic efficiency and current density for microbial fuel cells with different cathodes.

■ ASSOCIATED CONTENT

Supporting Information

Schematic diagram of the structure of carbon-constructed cathodes (Figure S1), equivalent circuit (Figure S2), nitrogen adsorption/desorption isotherms and pore size distribution of Fe_3O_4/GC-CS and Fe_3O_4/GC-PS obtained at different temperatures (Figures S3 and S4), linear sweep voltammetry curves (Figure S5), cyclic voltammetry current response for ORR (Figure S6), and voltage output of MFCs with different cathodes (Figure S7). This material is available free of charge via the Internet at http://pubs.acs.org/.

■ AUTHOR INFORMATION

Corresponding Authors

*E-mail: zoujinlong@aliyun.com. Phone: (+86)451 8660 8549. Fax: (+86) 451 8666 1259.
*E-mail: fuhg@vip.sina.com.

Notes

The authors declare no competing financial interest.

■ ACKNOWLEDGMENTS

We acknowledge support by the Key Program Projects of the National Natural Science Foundation of China (Grant 21031001), National Natural Science Foundation of China (Grants 51108162, 20971040, 51210105014, 21001042, 91122018, and 51102082), Natural Science Foundation of Heilongjiang Province (Grant B201411), Cultivation Fund of the Key Scientific and Technical Innovation Project, Ministry of Education of China (Grant 708029), Postdoctoral Science Foundation of China (Grants 2013T60395 and 20110491121) and Heilongjiang Province (Grant LBH-Z10048), Specialized Research Fund for the Doctoral Program of Higher Education of China (Grant 20112301110002), Research Project of the Educational Commission of Heilongjiang Province (Grants 11551338 and 12521450), and Youth Foundation of Heilongjiang University (Grant QL2010015).

■ REFERENCES

(1) Logan, B. E.; Hamelers, B.; Rozendal, R.; Schröder, U.; Keller, J.; Freguia, S.; Aelterman, P.; Verstraete, W.; Rabaey, K. Microbial Fuel Cells: Methodology and Technology. *Environ. Sci. Technol.* **2006**, *40*, 5181−5192.

(2) He, Z. Microbial Fuel Cells: Now Let Us Talk about Energy. *Environ. Sci. Technol.* **2012**, *47*, 332−333.
(3) Sonawane, J. M.; Gupta, A.; Ghosh, P. C. Multi-Electrode Microbial Fuel Cell (MEMFC): A Close Analysis towards Large Scale System Architecture. *Int. J. Hydrogen Energy* **2013**, *38*, 5106−5114.
(4) Kim, J. R.; Dec, J.; Bruns, M. A.; Logan, B. E. Removal of Odors from Swine Wastewater by Using Microbial Fuel Cells. *Appl. Environ. Microb.* **2008**, *74*, 2540−2543.
(5) Chen, X.; Liang, P.; Wei, Z. M.; Zhang, X. Y.; Huang, X. Sustainable Water Desalination and Electricity Generation in a Separator Coupled Stacked Microbial Desalination Cell with Buffer Free Electrolyte Circulation. *Bioresour. Technol.* **2012**, *119*, 88−93.
(6) Cusick, R. D.; Kim, Y.; Logan, B. E. Energy Capture from Thermolytic Solutions in Microbial Reverse-Electrodialysis Cells. *Science* **2012**, *335*, 1474−1477.
(7) Qu, L. T.; Liu, Y.; Baek, J.; Dai, L. M. Nitrogen-Doped Graphene as Efficient Metal-Free Electrocatalyst for Oxygen Reduction in Fuel cells. *ACS Nano* **2010**, *4*, 1321−1326.
(8) Stamenkovic, V. R.; Fowler, B.; Mun, B. S.; Wang, G.; Ross, P. N.; Lucas, C. A.; Markovic, N. M. Improved Oxygen Reduction Activity on $Pt_3Ni(111)$ via Increased Surface Site Availability. *Science* **2007**, *315*, 493−497.
(9) You, S. J.; Wang, X. H.; Zhang, J. N.; Wang, J. Y.; Ren, N. Q.; Gong, X. B. Fabrication of Stainless Steel Mesh Gas Diffusion Electrode for Power Generation in Microbial Fuel Cell. *Biosens. Bioelectron.* **2011**, *26*, 2142−2146.
(10) Xie, X.; Pasta, M.; Hu, L.; Yang, Y.; McDonough, J.; Cha, J.; Criddle, C. S.; Cui, Y. Nano-Structured Textiles as High-Performance Aqueous Cathodes for Microbial Fuel Cells. *Energy Environ. Sci.* **2011**, *4*, 1293−1297.
(11) Gong, K.; Du, F.; Xia, Z.; Durstock, M.; Dai, L. Nitrogen-Doped Carbon Nanotube Arrays with High Electrocatalytic Activity for Oxygen Reduction. *Science* **2009**, *323*, 760−764.
(12) Wu, Z. S.; Yang, S.; Sun, Y.; Parvez, K.; Feng, X.; Müllen, K. 3D Nitrogen-Doped Graphene Aerogel-Supported Fe_3O_4 Nanoparticles as Efficient Electrocatalysts for the Oxygen Reduction Reaction. *J. Am. Chem. Soc.* **2012**, *134*, 9082−9085.
(13) Feng, L.; Yan, Y.; Chen, Y.; Wang, L. Nitrogen-Doped Carbon Nanotubes as Efficient and Durable Metal-Free Cathodic Catalysts for Oxygen Reduction in Microbial Fuel Cells. *Energy Environ. Sci.* **2011**, *4*, 1892−1899.
(14) Roy, S.; Das, T.; Yue, C. Y.; Hu, X. Improved Polymer Encapsulation on Multiwalled Carbon Nanotubes by Selective Plasma Induced Controlled Polymer Grafting. *ACS Appl. Mater. Interfaces* **2014**, *6*, 664−670.
(15) Mattia, D.; Rossi, M. P.; Kim, B. M.; Korneva, G.; Bau, H. H.; Gogotsi, Y. Effect of Graphitization on the Wettability and Electrical Conductivity of CVD-Carbon Nanotubes and Films. *J. Phys. Chem. B* **2006**, *110*, 9850−9855.
(16) Sharma, S.; Sharma, A.; Cho, Y. K.; Madou, M. Increased Graphitization in Electrospun Single Suspended Carbon Nanowires Integrated with Carbon-MEMS and Carbon-NEMS Platforms. *ACS Appl. Mater. Interfaces* **2012**, *4*, 34−39.
(17) Su, Y.; Zhu, Y.; Yang, X.; Shen, J.; Lu, J.; Zhang, X.; Chen, J.; Li, C. A Highly Efficient Catalyst toward Oxygen Reduction Reaction in Neutral Media for Microbial Fuel Cells. *Ind. Eng. Chem. Res.* **2013**, *52*, 6076−6082.
(18) Hao Yu, E.; Cheng, S.; Scott, K.; Logan, B. E. Microbial Fuel Cell Performance with Non-Pt Cathode Catalysts. *J. Power Sources* **2007**, *171*, 275−281.
(19) Xia, X.; Zhang, F.; Zhang, X.; Liang, P.; Huang, X.; Logan, B. E. Use of Pyrolyzed Iron Ethylenediaminetetraacetic Acid Modified Activated Carbon as Air-Cathode Catalyst in Microbial Fuel Cells. *ACS Appl. Mater. Interfaces* **2013**, *5*, 7862−7866.
(20) Liu, H.; Logan, B. E. Electricity Generation Using an Air-Cathode Single Chamber Microbial Fuel Cell in the Presence and Absence of a Proton Exchange Membrane. *Environ. Sci. Technol.* **2004**, *38*, 4040−4046.
(21) Dong, H.; Yu, H.; Wang, X.; Zhou, Q.; Feng, J. A Novel Structure of Scalable Air-Cathode without Nafion and Pt by Rolling Activated Carbon and PTFE as Catalyst Layer in Microbial Fuel Cells. *Water Res.* **2012**, *46*, 5777−5787.
(22) Watson, V. J.; Delgado, C. N.; Logan, B. E. Influence of Chemical and Physical Properties of Activated Carbon Powders on Oxygen Reduction and Microbial Fuel Cell Performance. *Environ. Sci. Technol.* **2013**, *47*, 6704−6710.
(23) Wang, X.; Cheng, S. A.; Feng, Y. J.; Merrill, M. D.; Saito, T.; Logan, B. E. Use of Carbon Mesh Anodes and the Effect of Different Pretreatment Methods on Power Production in Microbial Fuel Cells. *Environ. Sci. Technol.* **2009**, *43*, 6870−6874.
(24) Wei, B.; Tokash, J. C.; Chen, G.; Hickner, M. A.; Logan, B. E. Development and Evaluation of Carbon and Binder Loading in Low-Cost Activated Carbon Cathodes for Air-Cathode Microbial Fuel Cells. *RSC Adv.* **2012**, *2*, 12751−12758.
(25) Zhang, X.; Xia, X.; Ivanov, I.; Huang, X.; Logan, B. E. Enhanced Activated Carbon Cathode Performance for Microbial Fuel Cell by Blending Carbon Black. *Environ. Sci. Technol.* **2014**, *48*, 2075−2081.
(26) Wang, S.; Zhang, L.; Xia, Z.; Roy, A.; Chang, D. W.; Baek, J. B.; Dai, L. BCN Graphene as Efficient Metal-Free Electrocatalyst for the Oxygen Reduction Reaction. *Angew. Chem., Int. Ed.* **2012**, *51*, 4209−4212.
(27) Obiuztsova, E. D.; Fujii, M.; Hayashi, S.; Kuznetsov, V. L.; Butenko, Y. V.; Chuvilin, A. L. Raman Identification of Onion-like Carbon. *Carbon* **1998**, *36*, 821−826.
(28) Lee, J. S.; Park, G. S.; Kim, S. T.; Liu, M.; Cho, J. A Highly Efficient Electrocatalyst for the Oxygen Reduction Reaction: N-Doped Ketjenblack Incorporated into Fe/Fe_3C-Functionalized Melamine Foam. *Angew. Chem.* **2013**, *125*, 1060−1064.
(29) Feng, L.; Chen, Y.; Chen, L. Easy-to-Operate and Low-Temperature Synthesis of Gram-Scale Nitrogen-Doped Graphene and Its Application as Cathode Catalyst in Microbial Fuel Cells. *ACS Nano* **2011**, *5*, 9611−9618.
(30) Meng, Q.; Zhang, F.; Wang, L.; Xiang, S.; Zhu, S.; Zhang, G.; Zhang, K.; Yang, B. Facile Fabrication of Mesoporous N-Doped Fe_3O_4@C Nanospheres as Superior Anodes for Li-Ion Batteries. *RSC Adv.* **2014**, *4*, 713−716.
(31) Wang, X.; Dai, Y.; Zou, J.; Meng, L.; Ishikawa, S.; Li, S.; Abuodeidah, M.; Fu, H. Characteristics and Antibacterial Activity of Ag-Embedded Fe_3O_4@SiO_2 Magnetic Composite as a Reusable Water Disinfectant. *RSC Adv.* **2013**, *3*, 11751−11758.
(32) Chen, G.; Wei, B.; Luo, Y.; Logan, B. E.; Hickner, M. A. Polymer Separators for High-Power, High-Efficiency Microbial Fuel Cells. *ACS Appl. Mater. Interfaces* **2013**, *4*, 6454−6457.
(33) Khilari, S.; Pandit, S.; Ghangrekar, M. M.; Pradhan, D.; Das, D. Graphene Oxide-Impregnated PVA−STA Composite Polymer Electrolyte Membrane Separator for Power Generation in a Single Chambered Microbial Fuel Cell. *Ind. Eng. Chem. Res.* **2013**, *52*, 11597−11606.
(34) Yuan, Y.; Zhou, S.; Tang, J. In Situ Investigation of Cathode and Local Biofilm Microenvironments Reveals Important Roles of OH^- and Oxygen Transport in Microbial Fuel Cells. *Environ. Sci. Technol.* **2013**, *47*, 4911−4917.
(35) Gong, X.; You, S.; Wang, X. H.; Zhang, J. N.; Gan, Y.; Ren, N. Q. A Novel Stainless Steel Mesh/Cobalt Oxide Hybrid Electrode for Efficient Catalysis of Oxygen Reduction in a Microbial Fuel Cell. *Biosens. Bioelectron.* **2014**, *55*, 237−241.
(36) Wen, Z.; Ci, S.; Zhang, F.; Feng, X.; Cui, S.; Mao, S.; Luo, S.; He, Z.; Chen, J. Nitrogen-Enriched Core−Shell Structured Fe/Fe_3C−C Nanorods as Advanced Electrocatalysts for Oxygen Reduction Reaction. *Adv. Mater.* **2012**, *24*, 1399−1404.
(37) Lu, M.; Guo, L.; Kharkwal, S.; Wu, H.; Ng, H. Y.; Li, S. F. Y. Manganese−Polypyrrole−Carbon Nanotube, a New Oxygen Reduction Catalyst for Air-Cathode Microbial Fuel Cells. *J. Power Sources* **2013**, *221*, 381−386.
(38) Zhang, F.; Pant, D.; Logan, B. E. Long-Term Performance of Activated Carbon Air Cathodes with Different Diffusion Layer

Porosities in Microbial Fuel Cells. *Biosens. Bioelectron.* **2011**, *30*, 49−55.
(39) Yu, H.; Dong, H.; Wang, X. Catalysis Kinetics and Porous Analysis of Rolling Activated Carbon−PTFE Air-Cathode in Microbial Fuel Cells. *Environ. Sci. Technol.* **2013**, *46*, 13009−13015.
(40) Liu, R.; Wu, D.; Feng, X.; Müllen, K. Nitrogen-Doped Ordered Mesoporous Graphitic Arrays with High Electrocatalytic Activity for Oxygen Reduction. *Angew. Chem.* **2010**, *122*, 2619−2623.